Published in final edited form as:
Circulation. 2013 September 10; 128(11 0 1): . doi:10.1161/CIRCULATIONAHA.112.000363.

A Reproducible Porcine Model of Thoracic Aortic Aneurysm

Shaina R. Eckhouse, MD[1], **Christina B. Logdon, MVT**[1], **J. Marshall Oelsen, BS**[1], **Risha K. Patel, BS**[1], **Allison D. Rice, BS**[1], **Robert E. Stroud, MS**[1], **W. Benjamin Wince, MD**[3], **Rupak Mukherjee, PhD**[1], **Francis G. Spinale, MD, PhD**[4], **John S. Ikonomidis, MD, PhD**[1], and **Jeffrey A. Jones, PhD**[1,2]

[1]Division of Cardiothoracic Surgery, Department of Surgery, Medical University of South Carolina

[2]Research Service, Ralph H. Johnson Veterans Affairs Medical Center, Medical University of South Carolina

[3]Division of Cardiology, Department of Medicine, Medical University of South Carolina

[4]Department of Cell Biology and Anatomy, University of South Carolina School of Medicine

Abstract

Background—Thoracic aortic aneurysms (TAAs) develop secondary to abnormal aortic extracellular matrix (ECM) remodeling, resulting in a weakened and dilated aortic wall that progressed to rupture if left unattended. Currently, no diagnostic/prognostic tests are available for detection of TAA disease. This is largely driven by the lack of a large animal model, which would permit longitudinal/mechanistic studies. Accordingly, the objective of the current study was to establish a reproducible porcine model of aortic dilatation, which recapitulates the structural and biochemical changes observed during human TAA development.

Methods and Results—Descending TAAs were induced in Yorkshire pigs (20–25 kg; n=7) through intra-adventitial injections of collagenase (5 ml, 0.35 mg/ml) and peri-adventitial application of crystalline $CaCl_2$ (0.5 g). Three weeks post-TAA induction, aortas were harvested and tissue was collected for biochemical and histological measurements. A subset of animals underwent magnetic resonance imaging pre-operatively and at terminal surgery. Results were compared to sham-operated controls (n=6). Three weeks post-TAA induction, aortic luminal area had increased 38±13% (p=0.018 vs. control). Aortic structural changes included elastic lamellar degradation and decreased collagen content. The protein abundance of MMPs -3, -8, -9, and -12 increased in TAA tissue homogenates, while TIMPs -1, and -4 decreased.

Conclusions—These data demonstrate aortic dilatation, aortic medial degeneration, and alterations in MMP/TIMP abundance, consistent with TAA formation. This study establishes for the first time, a large animal model of TAA that recapitulates the hallmarks of human disease, and will provide a reproducible test-bed for examining diagnostic, prognostic, and therapeutic strategies.

Address for Correspondence: Jeffrey A. Jones, Ph.D., Assistant Professor/Research Health Scientist, Medical University of South Carolina, Ralph H. Johnson VA Medical Center, Cardiothoracic Surgery Research, Strom Thurmond Research Building, 114 Doughty Street • Suite 326C, PO Box 250778, Charleston, SC 29425, Tel: (843) 792-0062, Fax: (843) 876-5187, jonesja@musc.edu.

Conflict of Interest Disclosures: Dr. Spinale is a grant recipient from NIH and the VA and serves as a consultant for Boston Scientific, Acorn Cardiovascular, and Roche Pharmaceuticals. Dr. Ikonomidis is a grant recipient from NIH and serves as a consultant for W.L. Gore and Associates, and On-X Life Technologies. Dr. jones is a grant recipient from the VA. The other authors report no conflicts.

Keywords

aortic disease; aneurysm; animal models of cardiovascular disease remodeling

Introduction

A thoracic aortic aneurysm (TAA) is defined as a localized dilatation to a diameter of greater than one and a half times normal in the supra-diaphragmatic aorta.[1–3] TAA development is influenced by a series of interrelated mechanisms that result in a weakened aortic wall and gross dilatation progressing to rupture if left untreated.[1, 4–9] Alarmingly, there are no diagnostic or prognostic tests currently available for detecting and tracking TAA disease. Typically, a TAA is diagnosed incidentally during a routine physical examination or during the work-up of another medical issue.[1–3] Furthermore, current therapeutic options are limited to high-risk open surgical repair or endovascular stent grafting, which is often constrained by the anatomical location of the TAA and is associated with procedure- and device-related complications. Even with surgical treatment, these approaches do not directly target the underlying cellular and molecular mechanisms that drive TAA development.

Thoracic aortic aneurysm development is multifactorial and results in degeneration of the aortic wall structure and composition, in part due to ECM remodeling. One mechanism that drives the pathological ECM remodeling process is the dysregulation of the matrix metalloproteinases (MMPs) and their endogenous tissue inhibitors (TIMPs).[1, 8, 10, 11] In the normal aorta, a stoichiometric balance exists between MMPs and TIMPs, keeping MMP activity tightly regulated. However, in TAA disease, this balance is disrupted favoring increased proteolysis and, leading to pathological remodeling of the aortic ECM. A second driving force in TAA development occurs due to alterations in the cellular constituents within the aortic wall. In clinical TAA specimens, infiltration of inflammatory cells in combination with the apoptotic loss of smooth muscle cells, contributes significantly to changes in aortic structure and function.[12–16] To further understand these changes and the mechanisms driving them, a murine model of TAA has been established, in which the application of calcium chloride to the periadventitial surface of the descending thoracic aorta resulted in progressive aortic dilatation and aortic wall remodeling, recapitulating key hallmarks of human aneurysmal disease.[17–23] Importantly, this model of TAA demonstrated alterations in the protein abundance of MMPs and TIMPs, favoring pathological ECM remodeling, and the emergence of a fibroblast-derived myofibroblast population concomitant with a loss of medial smooth muscle cells.[22, 23] While the murine model is advantageous for studying specific cellular and molecular mechanisms that influence TAA development, the physiologic, anatomic, and functional differences of the mouse aorta limit the translation of these findings to human application. Thus, it is important to bridge the gap between the extensive work performed in murine models and direct clinical application in humans,[24] through the development of a clinically relevant large animal model of TAA that will permit mechanistic as well as targeted therapeutic interventions. Therefore, the objective of the present study was to establish a reproducible porcine model of aortic dilatation, which recapitulates the structural and biochemical changes, observed in clinical disease.

Methods

Chronic Instrumentation

Yorkshire pigs (n=7, castrated males; weight: 20–25 kg; Hambone Farms, Orangeburg, SC) underwent sedation with intramuscular ketamine (22 mg/kg), placement of an intravenous

cannula in an ear vein, and endotracheal intubation followed an initiation of mechanical ventilation. A stable plane of anesthesia was maintained with isoflurane (2%, 3 L/min O_2, Baxter Healthcare Corp., Deerfield, IL), and a maintenance infusion of intravenous fluids (10 mL/kg, lactated Ringers) was begun. A postro-lateral left thoracotomy was performed based on the fourth intercostal space, and the proximal descending thoracic aorta was dissected from the surrounding tissue. The hemiazygous vein and two to three sets of the cranial-most intercostal arteries were ligated and divided where appropriate, creating a ~5 cm area of isolated descending thoracic aorta, centered on a line passing through the apex of the heart. Low-dose type-II bacterial collagenase (5 mL, 0.35 mg/mL in saline with 0.1 M $CaCl_2$; Cat. #LS004176, Worthington Biochemical Corp., Lakewood, NJ) was circumferentially injected intra-adventitially into the vascular wall of the isolated region. A piece of absorbable gelatin sponge (Gelfoam, Pharmacia Corp., Kalamazoo, MI) was cut to fit and slid under the mobilized aortic region. Dry powdered calcium chloride ($CaCl_2$, 0.5 g, 0.75 M equivalent, Cat. #C5080, Sigma-Aldrich Chemical Company, St. Louis, MO) was then circumferentially applied to the adventitial surface of the isolated segment of aorta. The Gelfoam was then wrapped around the aorta, enclosing the area of $CaCl_2$ application, to minimize irritation to the lung and heart. The chest was closed in layers, and the animals were allowed to recover. Results were compared to referent control animals (n=6), which did not receive collagenase injections or calcium chloride powder. All animals were treated and cared for in accordance with the National Institutes of Health *Guide for the Care and Use of Laboratory Animals* (Revised, 1996), and all protocols were approved by the Medical University of South Carolina's Institutional Animal Care and Use Committee.

Aortic Tissue Harvest

At the time of terminal surgery (n=6, 3-weeks post-TAA induction) the animals were sedated (diazepam, 200mg po), and isoflurane anesthesia was induced (5%, 1.5 L/min O_2). A median sternotomy was performed, and the ascending, arch, and descending aorta were harvested. The treatment region was carefully excised and cut into segments that were subsequently used for histological and biochemical analysis.

Aortic histological measurements

Two independent tissue segments from each aorta (n=6 TAA, n=6 control; separated by approximately 1.0 cm) were fixed in 10% formalin for 48 hours at 4°C, followed by 70% ethanol for 24 hours at 4°C. The pair of fixed tissue sections were then paraffin-embedded on end and 5 μm-thick cross-sections were cut and mounted on glass slides. The tissue sections were then deparaffinized, stained with hematoxylin and eosin (H&E; general structure), Verhoeff-Van Gieson (VVG, elastic architecture), and picrosirius red (PSR; collagen fibers). Microscopic images of aortic tissue sections were visualized on a Zeiss Axioskop 2 microscope (Carl Zeiss MicroImaging, Thornwood, NY) using a 63X/1.25 Plan-NEOFLUAR oil objective and acquired using an Axiocam MRc color charge-coupled device camera connected to a computer running AxioVision (v4.7). All subsequent image analysis was performed using SigmaScanPro v5.0 (SPSS, Chicago, IL). Collagen and elastin content was determined from the digitized images as a percentage of total tissue area in a minimum of 5 random high power fields from each aortic section for each pig using computer assisted morphometric methods. The number of elastic lamellae were counted from VVG stained sections.

Cellular constituents within the aortic media were identified and quantitated using immunohistochemical techniques with antibodies that recognized cell-type-specific marker proteins.[22] Tissue sections on slides were incubated in a citrate buffer for 30 minutes for antigen retrieval. The tissue sections were then incubated in blocking solution (3% bovine serum albumin in Tris-buffered saline wash solution) for 2 hours at room temperature,

followed by overnight incubation at 4°C with cell-type-specific primary antibodies diluted in blocking solution. Cell-type-specific antisera were used to identify: 1) fibroblasts (goat anti-discoidin domain receptor 2 (DDR2), 1:100, SC-7555; Santa Cruz Biotechnology, Santa Cruz, CA); 2) smooth muscle cells/myofibroblasts (rabbit anti-smooth muscle myosin heavy chain 2: Myh11), 1:100, ab53219; Abcam, Cambridge, MA); 3) smooth muscle cells/ myofibroblasts (rabbit anti-α-smooth-muscle actin (α-SMA), 1:100, ab2547; Abcam); 4) smooth muscle cells (rabbit anti-desmin, 1:20, D8281; Sigma-Aldrich, St. Louis, MO). The slides were then washed with PBS and incubated in 3% H2O2/PBS for 30 minutes at room temperature to block endogenous peroxidase activity. The sections were then allowed to incubate with primary antibody species-specific peroxidase-conjugated species-appropriate secondary antibodies (VectaStain, Vector Laboratories, Burlingame, CA). Positive immune reactions were visualized by incubating the sections with 0.05% diaminobenzidine, which formed a brown precipitate on reaction with the peroxidase enzyme. Serial sections were used for negative controls and were processed in the same fashion but without the addition of the primary antisera. The number of positively stained cells was counted from a minimum of 5 digitized images of high power fields (HPF) from each aortic section for each pig.

To calculate the aortic luminal cross-sectional area, four sections from two separate aortic segments of the treatment region were digitized (8 sections total per animal). The luminal area was digitally filled in, and area measurements were made using a calibrated (1 cm × 1 cm area) digital caliper. The measured aortic luminal area for each of the 8 sections was then averaged to calculate a mean aortic luminal area per aorta. A mean for each sample group, TAA group and control group, was then calculated and the results were expressed as a percent change from control.

MMP/TIMP Measurements

Immunoblotting

Aortic tissue (n=6 TAA, n=6 control) was transferred to cold extraction/homogenization buffer (buffer volume 1:6 w/v) containing 10 mM cacodylic acid pH 5.0, 0.15 M NaCl, 10 mM $ZnCl_2$, 1.5 mM NaN_3, and 0.01% Triton X-100 (v/v), and homogenized using the Qiagen Tissuelyser (Qiagen). The homogenate was centrifuged (800 × g, 10 min, 4°C) and 10 μg of the supernatant was loaded on a 4–12% bis-tris gradient gel and fractionated by electrophoresis. The proteins were then transferred to nitrocellulose membranes (0.45 μm, Bio-Rad) and incubated in antiserum (MMP-1, MMP-3, MMP-7, MMP-8, MMP-12, MMP-13, MT1-MMP, TIMP-1, TIMP-2, TIMP-3 and TIMP-4; *See* On-line Supplemental Materials and Table S1 *for details*) diluted in 5% non-fat dry milk/PBS. Species-specific secondary peroxidase conjugated antibody was then applied (1:5000, 5% non-fat dry milk/ PBS) and signals were detected with a chemiluminescent substrate (Western Lighting Chemiluminescence Reagent Plus, Perkin Elmer) and recorded on film. Band intensity was quantified using Gel-Pro Analyzer software (v3.1.14, Media Cybernetics Inc., Silver Spring, MD), and reported as a percent change from the unoperated reference control homogenates.

Gelatin Zymography

The relative abundance of MMP-2 and MMP-9 was assessed in the aortic tissue homogenates (n=6 TAA, n=6 control) by gelatin zymography. Aortic homogenates (10 μg protein) were fractionated on a non-denaturing 10% polyacrylamide gel containing 0.1% (w/ v) gelatin(Invitrogen Corporation, Carlsbad, CA). The gels were then equilibrated and incubated in Zymogram Developing Buffer (Invitrogen) for 18 hr at 37°C. After staining with 0.5% Coomassie Brilliant Blue (2 hr, room temperature), the gels were destained to reveal regions of gelatin clearance. The relative abundance of MMP-2 (as verified by a

recombinant MMP-2 standard) was then determined by densitometry using the Gel-Pro Analyzer software.

Computations and Data Analysis

Statistical analyses were performed using the STATA statistical software package (Statacorp v8.2, College Station, TX). For each comparison, the distribution of the continuous variables was tested using the Shapiro-Wilk normality test. All continuous variables were found to be normally distributed within each group. The values for luminal area, wall thickness, collagen/elastin ratio, the number of elastic lamellae, and the number of cells per HPF from histology sections (stained with DDR2, Myh11, desmin, and α-SMA) were compared between TAA and control animals using a two-tailed, two-sample mean comparison test. The percent change in relative protein abundance as determined by western blotting was examined using a two-tailed one-sample mean comparison test versus control (normal aorta set to a value of 100). Pairwise correlation analysis was performed to examine the relationships between MMP and TIMP abundance versus aortic luminal area. All results were presented as mean ± SEM and p-values of less than 0.05 were considered to be statistically significant.

Results

Surgical induction of TAA was uneventful with minimal peri-operative complications (Table S2). At three weeks following TAA induction, aortic dilation was evident upon gross examination. None of the TAA-induced animals experienced aortic rupture prior to terminal surgery. Dilatation started within the region of induction and would typically extend 1–2 cm beyond the distal most point of the treatment region. Significant wall thinning was grossly observed in aortic cross-sections in all TAA-induced animals versus referent controls (Figure 1A). Aortic luminal area, calculated from histological sections increased by 38±13% (p=0.018) in TAA-induced animals as compared to referent controls (*intra-assay CV:* TAA = 12.2%, Control = 12.2%; *inter-assay CV:* TAA = 16.6%, Control = 3.1%) (Figure 1B). In order to confirm aortic dilatation *in vivo*, the descending thoracic aorta was examined and aortic diameter measurements were made using a magnetic resonance imaging scanner (Siemens Magnetom Trio 3T, Germany). Electrocardiogram-gated two-dimensional dark-blood turbo spin-echo images, acquired during a single breath hold in a ventilated animal, were obtained under physiological hemodynamic loading conditions in one animal prior to surgical induction of TAA and at four weeks post-TAA induction. In this animal, aortic diameter was increased by 63.3% at 4 weeks post-TAA induction over the pre-induction baseline value (Figure 1C). Architectural changes in the aortic wall, consistent with TAA were observed. Specifically, aortic wall thickness (Figure 2A), the collagen to elastin ratio (Figure 2B), and the number of lamellar units (Figure 2C), as determined from histological sections, were decreased in the TAA group when compared to referent controls. These changes, in conjunction with the increase in aortic diameter, recapitulate the cross-sectional luminal dilation and loss of aortic wall architecture common in clinical TAA disease.

Changes in aortic cellular constituents were also evaluated following TAA induction (Figure 3). Specifically, a marker for aortic fibroblasts, DDR2 (Figure 3A–C), and a marker for myofibroblasts, Myh11 (Figure 3D–F), were both increased at three weeks post-TAA induction as compared to referent controls. In contrast, staining for desmin (Figure 3G–I), a marker for smooth muscle cells, and staining for α-smooth muscle actin, a marker expressed by both myofibroblasts and smooth muscle cells (Figure 3J–L), were reduced in the TAA specimens when compared to referent controls.

At the molecular level, the protein abundance of the ECM proteases (MMPs) and their endogenous inhibitors (TIMPs) were measured (Figure 4A–C). The abundance of active

MMP-2, MMP-3, MMP-8, MMP-9, MMP-12, and MT1-MMP were increased in TAA specimens versus referent controls. While no changes in MMP-1, MMP-7, or MMP-13 were observed. Conversely, the abundance of TIMP-1 and TIMP-4 were decreased as compared to referent controls, while no changes in TIMP-2 or TIMP-3 were observed. Pairwise correlation analysis revealed direct significant relationships between aortic luminal area and active MMP-2 abundance ($r=0.6149$, $p=0.033$) or MT1-MMP abundance ($r=0.5696$, $p=0.053$). Moreover, a trend towards an inverse relationship between aortic luminal area and TIMP-4 ($r=-0.5403$, $p=0.086$) was observed, but failed to reach statistical significance. Immunoblotting revealed that no residual type-II bacterial collagenase was detectable within the aortic tissue by the time of terminal study (Figure 4C).

Discussion

Thoracic aortic aneurysms (TAAs) develop secondary to abnormal extracellular matrix (ECM) remodeling, where alterations in activity of the matrix metalloproteinases (MMPs) and their endogenous inhibitors (TIMPs) favors increased proteolysis facilitating aortic wall thinning and dilatation. While numerous studies has been performed in wild-type and genetically modified murine models of TAA, and in clinical specimens obtained at the time of surgical intervention, the lack of a large animal model of TAA has limited the ability to perform serial mechanistic (serum/plasma testing) and interventional (device) studies at key points during TAA formation and progression. Thus, the objective of the present study was to establish a reproducible porcine model of aortic dilation which progresses to TAA, and to determine whether and to what degree the cellular and structural changes in the ECM would recapitulate the clinical disease phenotype. The unique findings of the present study were two-fold. First, this experimental methodology resulted in the reproducible dilatation of the descending thoracic aorta within three weeks post-TAA induction. Second, changes in aortic wall structure, cellular content, and protein abundance of MMPs and TIMPs in this porcine model, were consistent with the hallmarks of clinical TAA disease. Therefore, this large animal model of aortic dilatation may provide a reproducible test bed in which the development of diagnostic, prognostic, and therapeutic strategies can be examined for this devastating disease.

Thoracic aortic aneurysms form and progress through a multifactorial process involving both cellular and extracellular mechanisms. This process induces changes in the ECM composition and structure, over a prolonged period of time, and results in connective tissue degeneration and elastic fiber fragmentation within the aortic wall. Initiation and expansion of a descending TAA involves both hemodynamic factors, such as high blood pressure correlating to increased aortic wall tension,[25] and enhanced localized proteolysis within the aortic wall, leading to a weakening of the structural framework. Together these changes result in reduced aortic resilience and compliance, and enhance the propensity for catastrophic aortic rupture.

In the present study, the combination of intra-adventitial injections of low dose type-II bacterial collagenase and peri-adventitial exposure to $CaCl_2$ powder, was used to induce experimental TAAs in swine. The study demonstrated that this treatment protocol reproducibly induced a process that resulted in the dilatation of the descending thoracic aorta, consistent with that of aneurysm formation. When aortic geometry was assessed, either by examination of aortic intraluminal area from histological sections (demonstrating approx. 40% increase in intraluminal area at 3-wks post-TAA induction), or cross-sectional diameter at the widest part of the aneurysm measured by magnetic resonance imaging (demonstrating approx. 60% increase in diameter at 4-wks post-TAA-induction), both measurements confirmed significant aortic dilatation. This increase in dilatation was accompanied by significant thinning of the aortic wall, resulting from the fragmentation of

elastin, and a decrease in the number of intact elastic lamellar units. Moreover, in addition to the loss of elastin content, the ratio of collagen to elastin was also decreased, suggesting significant proteolysis of the surrounding collagen matrix.

To date, no large animal model of TAA has been described. Conversely, several large animal models (rabbit, swine) have previously been developed for the study of abdominal aortic aneurysms (AAA).[26–29] While there have been variable results in regard to the amount of aortic dilatation achieved, porcine models of AAA utilizing pancreatic elastase have demonstrated collagen and elastic degradation with an associated increase in MMP production.[26, 28, 29] In a rabbit model of AAA, adventitial application of calcium chloride along with a high cholesterol diet and the induction of adventitial inflammation caused a doubling of the aortic diameter in three weeks.[27] However, because of the regional heterogeneity between the thoracic and abdominal aorta, great caution should be taken when interpreting results from experimental models of AAA with regard to the thoracic aorta and TAA disease. Variations in embryonic cellular origin, atherosclerotic burden, degree of inflammatory infiltration, protease profiles, and vessel mechanics complicate direct comparisons.[30] Thus, the present study built on these past experiences in order to develop a reproducible model of TAA in swine.

It is now widely accepted that changes in aortic vascular structure and geometry occur during TAA development and are mediated in part by alterations in the abundance of a family of ECM proteolytic enzymes, the MMPs, and their endogenous tissue inhibitors, the TIMPs. The TIMPs bind to the MMPs in a 1:1 stoichiometric ratio and inhibit MMP activity.[10] Under normal conditions MMP and TIMP abundance is balanced; however, in the presence of TAA, this balance is disrupted in favor of proteolysis. Previous studies, from our group and others, using clinical TAA specimens have demonstrated this imbalance leading to enhanced proteolysis.[31–37] For example, Wilson and co-workers demonstrated the MMP-8 abundance was increased while TIMP-1 abundance was decreased.[37] Similarly, Koullias *et al.* demonstrated that the ratio of MMP-9 to TIMP-1 abundance was increased in TAA versus control specimens, suggesting that the aneurysm was in an enhanced proteolytic state.[35] The present study demonstrated a general increase in MMP abundance that was accompanied by a general decrease in TIMP abundance. This suggests an overall shift in the stoichiometric balance between these key mediators, favoring a more proteolytic phenotype. Moreover, significant relationships were identified between aortic luminal area and the increase in MMP abundance (MMP-2 and MT1-MMP) and an inverse trend was identified in relation to the decrease in TIMP abundance (TIMP-4). Together, these data suggest that elevated proteolysis likely drives aneurysm development in this model.

Since the harvest of clinical TAA tissue specimens is restricted to the time of surgical intervention, information regarding mechanisms that contribute to TAA formation and progression has been severely limited. As such, *in vivo* studies have been confined to murine models of TAA in an effort to explore the mechanisms involved in the formation and progression of disease.[20, 38] With respect to TAA disease, the murine models replicate many of the structural and biochemical hallmarks seen in clinical specimens. For example, histological characterization of a murine model of TAA demonstrated a decrease in the number of lamellae within the aortic wall and progressive disruption of the elastic architecture with progressive dilation, increased wall stiffness, as calculated by the ratio of total collagen area to total elastin ratio.[22] In addition to structural changes, murine models of TAA have provided evidence that changes in MMP and TIMP abundance occur concomitantly with the progression of TAA disease.[17, 20, 21, 23, 39] Transgenic studies demonstrated the importance of several MMPs and TIMPs in the process of ECM proteolysis leading to aortic dilatation. Specifically, in mice deficient for TIMP-1, TAA development was accelerated compared to wild-type animals,[19] while in mice deficient for

MMP-9, TAA development was attenuated.[18] Importantly, studies of TAA progression in MMP-9 reporter mice demonstrated that MMP-9 gene promoter activation was localized to fibroblasts within the aortic wall, suggesting that fibroblast cell lineage may play an important role in TAA formation and progression.[21] This was supported by a recent study demonstrating that concurrent with the apoptotic loss of aortic smooth muscle cells, there was an increase in fibroblasts and fibroblast-derived cells following TAA induction. Cell-type specific marker measurements were made for fibroblasts (DDR2), smooth muscle cells (desmin), and myofibroblasts (α-SMA and Myh11) within aortic tissue sections following TAA induction.[22] Interestingly, DDR2 and Myh11 concomitantly increased, while desmin decreased, and α-SMA remained unchanged. Taken together, these data suggested that in addition to the geometric and structural changes induced during TAA development, dynamic changes in the aortic cellular constituents also occur. These changes are characterized by the emergence of a fibroblast-derived myofibroblast population, positive for DDR2, Myh11, and α-SMA, concurrent with a decrease in desmin-positive aortic smooth muscle cells. Importantly, these alterations in the cellular constituents likely play an integral role in TAA formation and progression, by mediating changes in protease abundance and ECM protein production.

In the present study, the cellular constituents were measured in aortic tissue sections from pigs 3-weeks post-TAA induction and demonstrated increased staining for DDR2 and Myh11, concomitant with decreased staining for desmin and α-SMA. These results suggested that the changes in aortic cellular constituents during TAA development in pigs, may also be mediated in part by the formation of fibroblast-derived myofibroblasts, capable of directing the ECM remodeling process. Thus, this porcine model of TAA may be useful in further elucidating the mechanisms of cellular phenotype change and the role of fibroblast-derived cells in mediating aneurysm formation and progression.

The present study is not without limitations. First, due to the lack of a reproducible noninvasive method for measuring aortic diameter at baseline (prior to surgical TAA induction), a referent control group was used to establish normal intraluminal areas, as well as biochemical outcomes. Second, the change in aortic intraluminal area was measured at 3-weeks post-TAA induction on fixed histological sections. These measurements may actually under-represent the change in maximal aortic diameter observed following TAA induction. The use of magnetic resonance imaging (MRI) provides a high-resolution method for anatomical measurements in live animals. When used in this study, MRI demonstrated that aortic dilatation increased by more than 60% at 4-weeks post-TAA induction compared to baseline measurements obtained from the same animal prior to TAA-induction. Third, because aortic measurements were obtained following terminal surgery at a single time-point post-TAA induction (3-weeks), whether and to what degree aortic dilatation progresses over time, remains to be determined and will be addressed in future studies. Fourth, as previously identified in the mouse TAA model, calcium chloride can induce significant lung injury.[20] To improve on previous methods, dry calcium chloride powder (0.75 M equivalent) was applied to the peri-adventitial surface of the thoracic aorta and wrapped in gel foam in order to segregate the calcium chloride treated aorta from the lungs. While at terminal procedure, it was identified that the left lung was strongly adherent to the operative region, no lung necrosis or other gross changes were noted. All animals within the present study remained normoxic throughout the time course of the study as measured by pulse oximetry (data not shown). Lastly, while significant relationships exist between aortic size and changes in MMP/TIMP abundance, causality cannot be assumed; future studies intervening in the proteolytic pathway will be required.

These limitations notwithstanding, the present study demonstrated the creation of a novel and reproducible model of TAA development in swine, which recapitulates the structural,

histological, and biochemical changes attributed to human TAA disease. The use of this model will be highly valuable for device and serial blood testing, and may provide insight into potential new diagnostic, prognostic, and therapeutic approaches for this serious disease.

Supplementary Material

Refer to Web version on PubMed Central for supplementary material.

Acknowledgments

SRE was the recipient of the 2012 Vivien Thomas Young Investigator Award, presented at the 2012 Scientific Sessions Meeting of the American Heart Association.

Funding Sources: SRE was supported by an NIH National Research Service Award (T32 HL007260). This study was funded by the Cardiovascular Translation Research Center and the Division of Cardiothoracic Surgery, at the Medical University of South Carolina.

References

1. Barbour JR, Spinale FG, Ikonomidis JS. Proteinase systems and thoracic aortic aneurysm progression. J Surg Res. 2007; 139:292–307. [PubMed: 17292415]
2. Coady MA, Rizzo JA, Goldstein LJ, Elefteriades JA. Natural history, pathogenesis, and etiology of thoracic aortic aneurysms and dissections. Cardiol Clin. 1999; 17:615–635. [PubMed: 10589336]
3. Elefteriades JA. Natural history of thoracic aortic aneurysms: Indications for surgery, and surgical versus nonsurgical risks. Ann Thorac Surg. 2002; 74:S1877–S1880. discussion S1892-1878. [PubMed: 12440685]
4. Chiesa R, Melissano G, Civilini E, de Moura ML, Carozzo A, Zangrillo A. Ten years experience of thoracic and thoracoabdominal aortic aneurysm surgical repair: Lessons learned. Ann Vasc Surg. 2004; 18:514–520. [PubMed: 15534729]
5. Davies RR, Goldstein LJ, Coady MA, Tittle SL, Rizzo JA, Kopf GS, Elefteriades JA. Yearly rupture or dissection rates for thoracic aortic aneurysms: Simple prediction based on size. Ann Thorac Surg. 2002; 73:17–27. discussion 27-18. [PubMed: 11834007]
6. Fleck TM, Koinig H, Czerny M, Hutschala D, Wolner E, Ehrlich M, Grabenwoger M. Impact of surgical era on outcomes of patients undergoing elective atherosclerotic ascending aortic aneurysm operations. Eur J Cardiothorac Surg. 2004; 26:342–347. [PubMed: 15296894]
7. Ghansah JN, Murphy JT. Complications of major aortic and lower extremity vascular surgery. Semin Cardiothorac Vasc Anesth. 2004; 8:335–361. [PubMed: 15583793]
8. Isselbacher EM. Thoracic and abdominal aortic aneurysms. Circulation. 2005; 111:816–828. [PubMed: 15710776]
9. Kawaharada N, Morishita K, Fukada J, Hachiro Y, Fujisawa Y, Saito T, Kurimoto Y, Abe T. Stroke in surgery of the arteriosclerotic descending thoracic aortic aneurysms: Influence of cross-clamping technique of the aorta. Eur J Cardiothorac Surg. 2005; 27:622–625. [PubMed: 15784361]
10. Visse R, Nagase H. Matrix metalloproteinases and tissue inhibitors of metalloproteinases: Structure, function, and biochemistry. Circ Res. 2003; 92:827–839. [PubMed: 12730128]
11. Woessner JF Jr. Mmps and timps. An historical perspective. Methods Mol Biol. 2001; 151:1–23. [PubMed: 11217295]
12. Della Corte A, Quarto C, Bancone C, Castaldo C, Di Meglio F, Nurzynska D, De Santo LS, De Feo M, Scardone M, Montagnani S, Cotrufo M. Spatiotemporal patterns of smooth muscle cell changes in ascending aortic dilatation with bicuspid and tricuspid aortic valve stenosis: Focus on cell-matrix signaling. J Thorac Cardiovasc Surg. 2008; 135:8–18. 18 e11–12. [PubMed: 18179910]
13. He R, Guo DC, Estrera AL, Safi HJ, Huynh TT, Yin Z, Cao SN, Lin J, Kurian T, Buja LM, Geng YJ, Milewicz DM. Characterization of the inflammatory and apoptotic cells in the aortas of

patients with ascending thoracic aortic aneurysms and dissections. J Thorac Cardiovasc Surg. 2006; 131:671–678. [PubMed: 16515922]

14. Ihling C, Szombathy T, Nampoothiri K, Haendeler J, Beyersdorf F, Uhl M, Zeiher AM, Schaefer HE. Cystic medial degeneration of the aorta is associated with p53 accumulation, bax upregulation, apoptotic cell death, and cell proliferation. Heart. 1999; 82:286–293. [PubMed: 10455077]
15. Lopez-Candales A, Holmes DR, Liao S, Scott MJ, Wickline SA, Thompson RW. Decreased vascular smooth muscle cell density in medial degeneration of human abdominal aortic aneurysms. Am J Pathol. 1997; 150:993–1007. [PubMed: 9060837]
16. Thompson RW, Liao S, Curci JA. Vascular smooth muscle cell apoptosis in abdominal aortic aneurysms. Coron Artery Dis. 1997; 8:623–631. [PubMed: 9457444]
17. Barbour JR, Stroud RE, Lowry AS, Clark LL, Leone AM, Jones JA, Spinale FG, Ikonomidis JS. Temporal disparity in the induction of matrix metalloproteinases and tissue inhibitors of metalloproteinases after thoracic aortic aneurysm formation. J Thorac Cardiovasc Surg. 2006; 132:788–795. [PubMed: 17000289]
18. Ikonomidis JS, Barbour JR, Amani Z, Stroud RE, Herron AR, McClister DM Jr, Camens SE, Lindsey ML, Mukherjee R, Spinale FG. Effects of deletion of the matrix metalloproteinase 9 gene on development of murine thoracic aortic aneurysms. Circulation. 2005; 112:I242–I248. [PubMed: 16159824]
19. Ikonomidis JS, Gibson WC, Butler JE, McClister DM, Sweterlitsch SE, Thompson RP, Mukherjee R, Spinale FG. Effects of deletion of the tissue inhibitor of matrix metalloproteinases-1 gene on the progression of murine thoracic aortic aneurysms. Circulation. 2004; 110:II268–II273. [PubMed: 15364874]
20. Ikonomidis JS, Gibson WC, Gardner J, Sweterlitsch S, Thompson RP, Mukherjee R, Spinale FG. A murine model of thoracic aortic aneurysms. J Surg Res. 2003; 115:157–163. [PubMed: 14572787]
21. Jones JA, Barbour JR, Lowry AS, Bouges S, Beck C, McClister DM Jr, Mukherjee R, Ikonomidis JS. Spatiotemporal expression and localization of matrix metalloproteinas-9 in a murine model of thoracic aortic aneurysm. J Vasc Surg. 2006; 44:1314–1321. [PubMed: 17145436]
22. Jones JA, Beck C, Barbour JR, Zavadzkas JA, Mukherjee R, Spinale FG, Ikonomidis JS. Alterations in aortic cellular constituents during thoracic aortic aneurysm development: Myofibroblast-mediated vascular remodeling. Am J Pathol. 2009; 175:1746–1756. [PubMed: 19729479]
23. Jones JA, Zavadzkas JA, Chang EI, Sheats N, Koval C, Stroud RE, Spinale FG, Ikonomidis JS. Cellular phenotype transformation occurs during thoracic aortic aneurysm development. J Thorac Cardiovasc Surg. 2010; 140:653–659. [PubMed: 20219212]
24. Butler D. Translational research: Crossing the valley of death. Nature. 2008; 453:840–842. [PubMed: 18548043]
25. Ruddy JM, Jones JA, Stroud RE, Mukherjee R, Spinale FG, Ikonomidis JS. Differential effects of mechanical and biological stimuli on matrix metalloproteinase promoter activation in the thoracic aorta. Circulation. 2009; 120:S262–S268. [PubMed: 19752377]
26. Boyle JR, McDermott E, Crowther M, Wills AD, Bell PR, Thompson MM. Doxycycline inhibits elastin degradation and reduces metalloproteinase activity in a model of aneurysmal disease. J Vasc Surg. 1998; 27:354–361. [PubMed: 9510291]
27. Freestone T, Turner RJ, Higman DJ, Lever MJ, Powell JT. Influence of hypercholesterolemia and adventitial inflammation on the development of aortic aneurysm in rabbits. Arterioscler Thromb Vasc Biol. 1997; 17:10–17. [PubMed: 9012631]
28. Hynecek RL, DeRubertis BG, Trocciola SM, Zhang H, Prince MR, Ennis TL, Kent KC, Faries PL. The creation of an infrarenal aneurysm within the native abdominal aorta of swine. Surgery. 2007; 142:143–149. [PubMed: 17689678]
29. Marinov GR, Marois Y, Paris E, Roby P, Formichi M, Douville Y, Guidoin R. Can the infusion of elastase in the abdominal aorta of the yucatan miniature swine consistently produce experimental aneurysms? Journal of investigative surgery. 1997; 10:129–150. [PubMed: 9219089]

30. Ruddy JM, Jones JA, Spinale FG, Ikonomidis JS. Regional heterogeneity within the aorta: Relevance to aneurysm disease. J Thorac Cardiovasc Surg. 2008; 136:1123–1130. [PubMed: 19026791]

31. Boyum J, Fellinger EK, Schmoker JD, Trombley L, McPartland K, Ittleman FP, Howard AB. Matrix metalloproteinase activity in thoracic aortic aneurysms associated with bicuspid and tricuspid aortic valves. J Thorac Cardiovasc Surg. 2004; 127:686–691. [PubMed: 15001896]

32. Ikonomidis JS, Jones JA, Barbour JR, Stroud RE, Clark LL, Kaplan BS, Zeeshan A, Bavaria JE, Gorman JH 3rd, Spinale FG, Gorman RC. Expression of matrix metalloproteinases and endogenous inhibitors within ascending aortic aneurysms of patients with marfan syndrome. Circulation. 2006; 114:I365–I370. [PubMed: 16820601]

33. Ikonomidis JS, Jones JA, Barbour JR, Stroud RE, Clark LL, Kaplan BS, Zeeshan A, Bavaria JE, Gorman JH 3rd, Spinale FG, Gorman RC. Expression of matrix metalloproteinases and endogenous inhibitors within ascending aortic aneurysms of patients with bicuspid or tricuspid aortic valves. J Thorac Cardiovasc Surg. 2007; 133:1028–1036. [PubMed: 17382648]

34. Ikonomidis JS, Ruddy JM, Benton SM Jr, Arroyo J, Brinsa TA, Stroud RE, Zeeshan A, Bavaria JE, Gorman JH 3rd, Gorman RC, Spinale FG, Jones JA. Aortic dilatation with bicuspid aortic valves: Cusp fusion correlates to matrix metalloproteinases and inhibitors. Ann Thorac Surg. 2012; 93:457–463. [PubMed: 22206960]

35. Koullias GJ, Ravichandran P, Korkolis DP, Rimm DL, Elefteriades JA. Increased tissue microarray matrix metalloproteinase expression favors proteolysis in thoracic aortic aneurysms and dissections. Ann Thorac Surg. 2004; 78:2106–2110. discussion 2110-2101. [PubMed: 15561045]

36. LeMaire SA, Wang X, Wilks JA, Carter SA, Wen S, Won T, Leonardelli D, Anand G, Conklin LD, Wang XL, Thompson RW, Coselli JS. Matrix metalloproteinases in ascending aortic aneurysms: Bicuspid versus trileaflet aortic valves. J Surg Res. 2005; 123:40–48. [PubMed: 15652949]

37. Wilson WR, Schwalbe EC, Jones JL, Bell PR, Thompson MM. Matrix metalloproteinase 8 (neutrophil collagenase) in the pathogenesis of abdominal aortic aneurysm. Br J Surg. 2005; 92:828–833. [PubMed: 15918165]

38. Daugherty A, Rateri DL, Charo IF, Owens AP, Howatt DA, Cassis LA. Angiotensin ii infusion promotes ascending aortic aneurysms: Attenuation by ccr2 deficiency in apoe−/− mice. Clin Sci (Lond). 2010; 118:681–689. [PubMed: 20088827]

39. Jones JA, Ruddy JM, Bouges S, Zavadzkas JA, Brinsa TA, Stroud RE, Mukherjee R, Spinale FG, Ikonomidis JS. Alterations in membrane type-1 matrix metalloproteinase abundance after the induction of thoracic aortic aneurysm in a murine model. Am J Physiol Heart Circ Physiol. 2010; 299:H114–H124. [PubMed: 20418476]

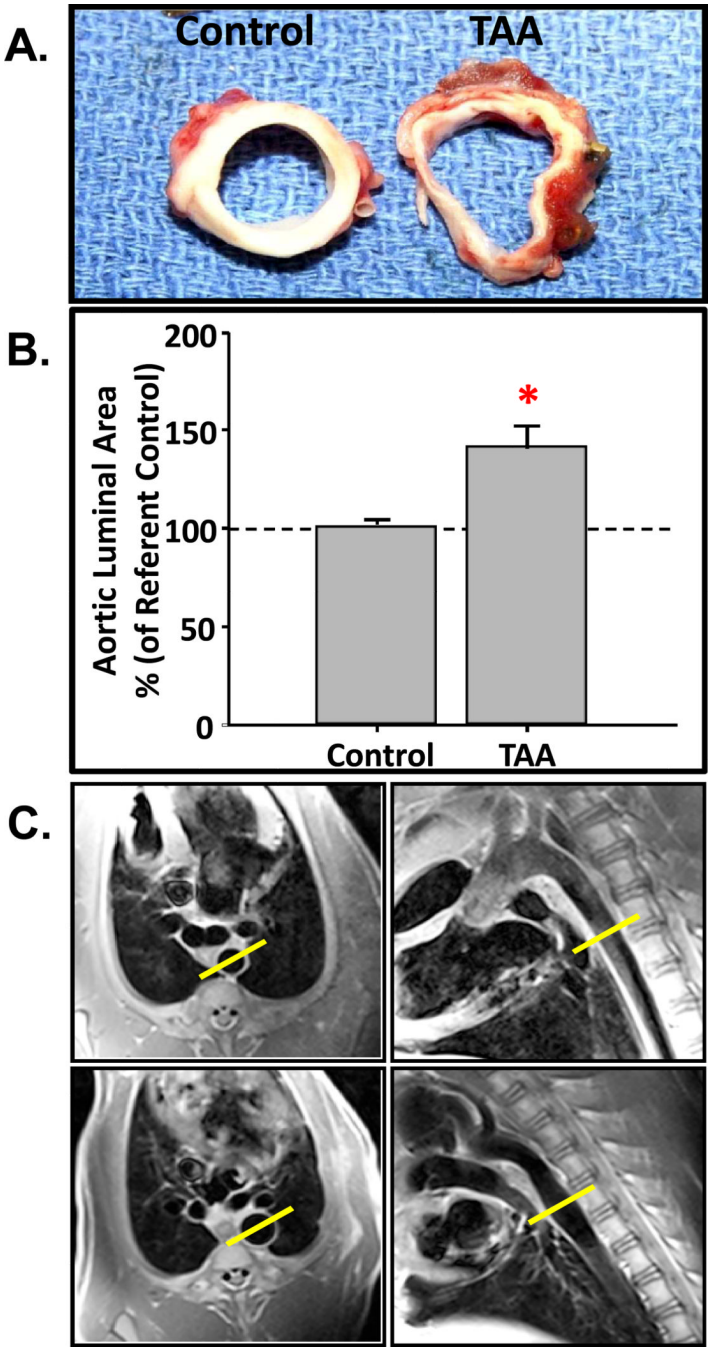

Figure 1.

Changes in aortic geometry post-TAA induction. ***A)*** Cross-sections of descending aortic tissue obtained from normal (left) and TAA-induced (right) pigs. ***B)*** The percent change in aortic luminal area was determined from histological sections obtained at 3-weeks post-TAA induction (n=6) and compared to referent controls (n=6). Aortic diameter increased by 38±13% (*, p=0.018 versus control). ***C)*** Magnetic resonance imaging of the descending thoracic aorta prior to (top) and 4-weeks after TAA induction (bottom). Short axis views (left panels) and sagittal views (right panels) were recorded at 4-weeks post-TAA induction. Aortic diameter was measured at the widest part of the aneurysm (17.8mm) and

demonstrated a 63.3% increase over pre-induction baseline (10.9mm), obtained in the same animal.

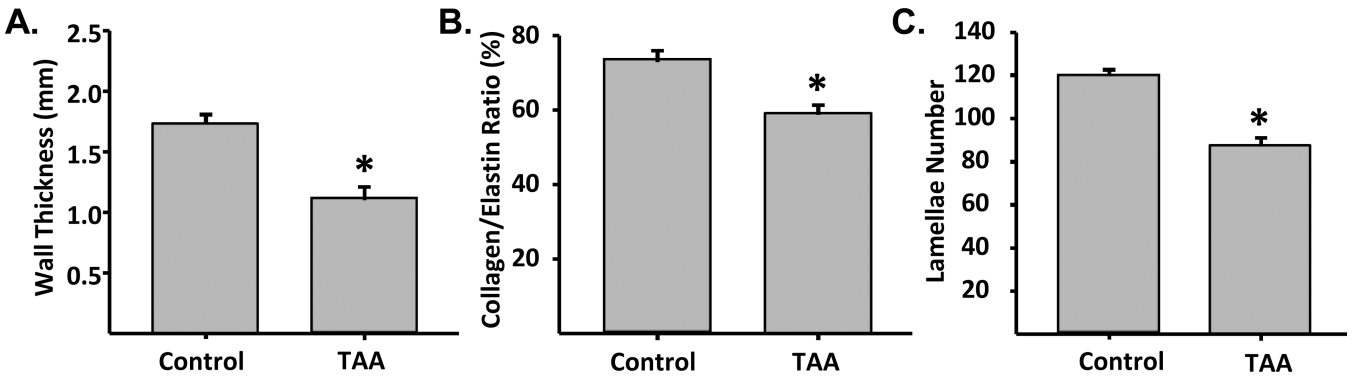

Figure 2.

Quantification of architectural changes induced with TAA. Morphometric changes in tissue architecture were quantified from stained histological sections to measure: ***A)*** aortic wall thickness (*, p=0.001), ***B)*** collagen/elastin ratio (*, p=0.004), and ***C)*** transmural lamellar number (*, p<0.001). Two independent sections from each aorta (n=6 TAA, n=6 control) were imaged and quantitated for each group. Wall thickness, collagen/elastin ratio, and lamellar number, were all significantly decreased in TAA sections as compared to reference controls.

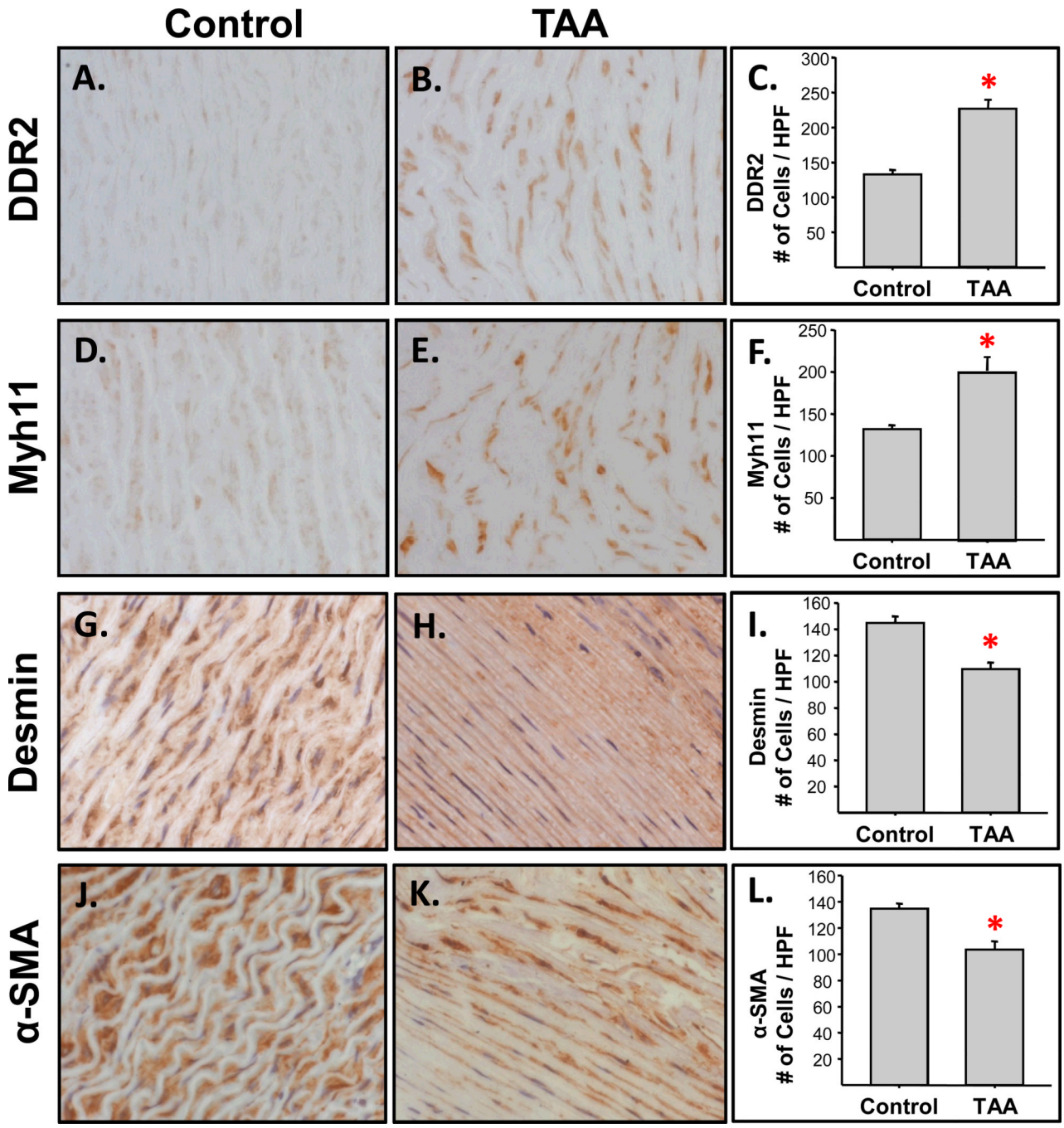

Figure 3.

Assessment of cellular changes during TAA formation. Two independent tissue segments from each aorta (n=6 TAA, n=6 control; separated by approximately 1.0 cm) were fixed, paraffin-embedded on end, cut in cross-section (5 μm-thick), and mounted on glass slides. The tissue sections were then stained for cell-type specific markers. Digital images from multiple high-power fields were quantitated using morphometric techniques. ***A–C)*** The fibroblast-specific marker, DDR2, was increased significantly in the TAA tissue sections as compared to referent controls (*, $p<0.001$); ***D–F)*** Myosin heavy chain-11, a marker for myofibroblasts, was significantly increased in the TAA tissues as compared to referent

controls (*, p=0.003); ***G–I)*** Staining for Desmin, a smooth muscle cell-specific marker, was decreased in the TAA tissue sections compared to the referent controls (*, p<0.001); ***J–L)*** Staining of α-smooth muscle actin (α-SMA), a marker for both smooth muscle cells and myofibroblasts, was also decreased in the TAA tissue sections as compared to referent controls (*, p=0.002).

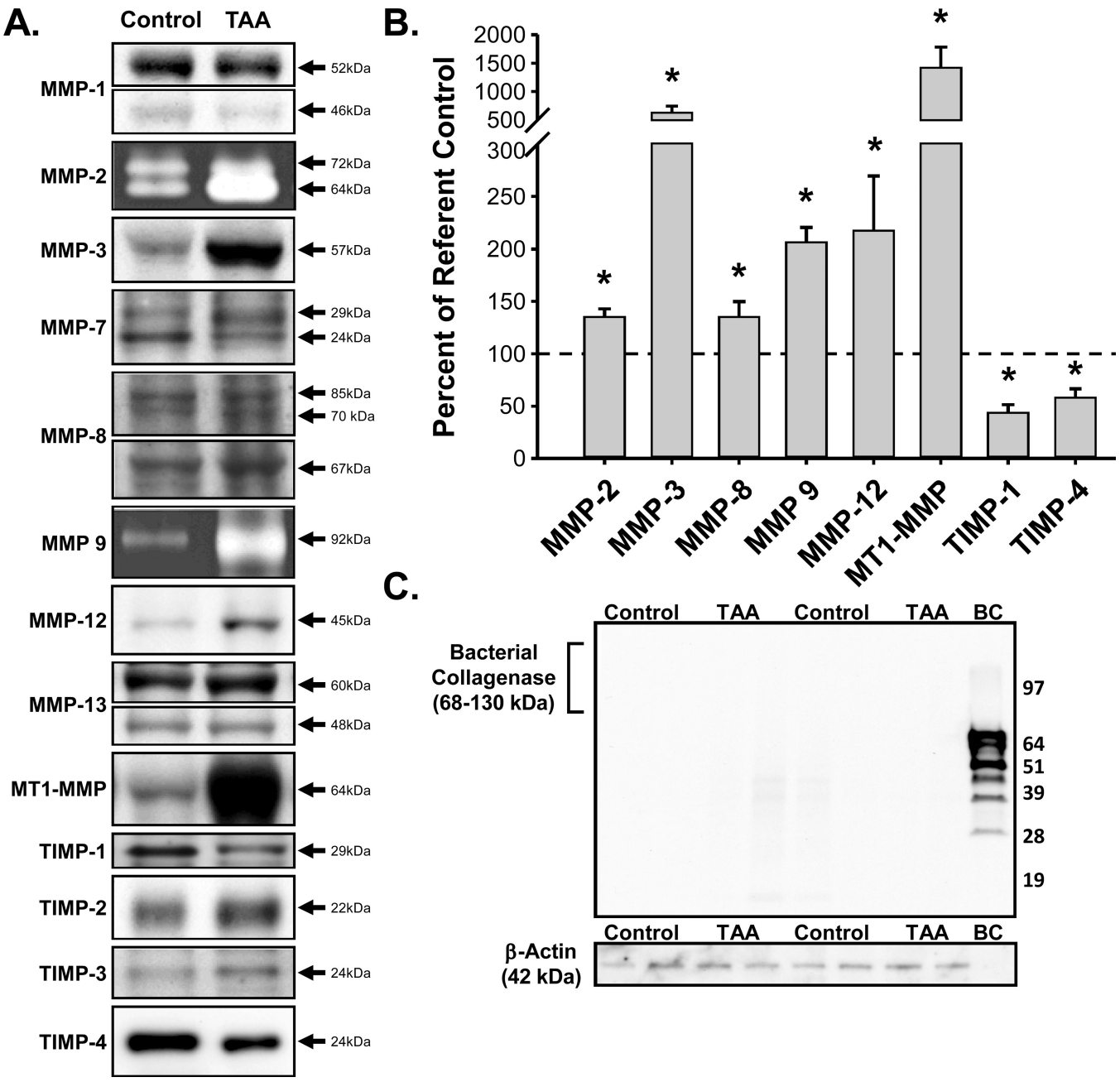

Figure 4.

Quantitation of MMP and TIMP protein abundance. ***A)*** Representative immunoblots for MMPs -1, -2, -3, -7, 8, -9, -12, -13, -14 (MT1-MMP), and TIMPs -1, -2, -3, and -4 from normal and TAA-induced aortic tissue homogenates. ***B)*** Summary of significant changes (*) in MMP and TIMP protein abundance in TAA tissue homogenates (n=6) as compared to referent controls (n=6). The abundance of active MMP-2 (p=0.009), MMP-3 (p=0.007), MMP-8 (p=0.043), MMP-9 (p=0.002), MMP-12 (p=0.040), and MT1-MMP (p=0.016) were increased, while the abundance of TIMP-1 (p=0.001) and TIMP-4 (p=0.010) were decreased in TAA specimens as compared to referent controls. ***C)*** Representative immunoblots for type-II bacterial collagenase and loading control, β-actin, in TAA tissue homogenates (n=4)

and referent controls (n=4). No residual bacterial collagenase was detected in the TAA tissue homogenates.